Control of Biofilm Formation by an *Agrobacterium tumefaciens* Pterin-Binding Periplasmic Protein Conserved Among Pathogenic Bacteria

Jennifer L. Greenwich[a], Justin L. Eagan[a], Nathan Feirer[a], Kaleb Boswinkle[b], George Minasov[c,d], Ludmilla Shuvalova[e], Nicole L. Inniss[c,d], Jakka Raghavaiah[f], Arun K. Ghosh[f], Karla J.F. Satchell[c,d], Kylie D. Allen[b] and Clay Fuqua[a]*

[a]Department of Biology
Indiana University
Bloomington, IN 47405 USA

[b]Department of Biochemistry
Virginia Polytechnic Institute and State University
Blacksburg, VA 24061 USA

[c]Department of Microbiology-Immunology
Feinberg School of Medicine
Northwestern University
Chicago, IL 60611 USA

[d]Center for Structural Biology of Infectious Diseases
Feinberg School of Medicine
Northwestern University
Chicago, IL 60611 USA

[e]Department of Pharmacology
Feinberg School of Medicine
Northwestern University
Chicago, IL 60611 USA

[f]Departments of Chemistry and Medicinal Chemistry
Purdue University
West Lafayette, IN 47907 USA

[*]Clay Fuqua
E-mail: cfuqua@indiana.edu

Current addresses: J.L.E., Medical Microbiology and Immunology, University of Wisconsin, Madison, WI 53706; N.F., Promega Corp., Madison, WI, 53711

Author contributions: J.L.G, J.L.E., K.D.A. and C.F. designed the study; J.L.G., J.L.E., N.F., and K.B. performed the genetic and microbiological experiments, and J.L.G., K.B. and K.D.A. performed biochemical analysis of pterins and pterin-binding. L.S. and G.M. performed crystallization and structural determination. J.R. and A.K.G. developed and implemented a new pterin synthesis method. J.L.G., K.D.A., N.L.I., G.M. K.J.S.F. and C.F wrote the manuscript with input from all authors. C.F. supervised the entire study.

Competing Interest Statement: K.J.F.S. has a significant interest in Situ Biosciences, a contract research organization that conducts research unrelated to this study. All other authors declare no conflicts of interest. The funders had no role in study design, data collection, and analysis, decision to publish, or preparation of the manuscript.

Classification: Biological Sciences/Microbiology
Keywords: Biofilm, regulation, pterin, cyclic duguanylate monophosphate, protein structure

This PDF file contains: Main text (6766 words), Figures 1-7, Supplementary Information

ABSTRACT

Biofilm formation and surface attachment in multiple Alphaproteobacteria is driven by unipolar polysaccharide (UPP) adhesins. The pathogen *Agrobacterium tumefaciens* produces a UPP adhesin, which is regulated by the intracellular second messenger cyclic diguanylate monophosphate (cdGMP). Prior studies revealed that DcpA, a diguanylate cyclase-phosphodiesterase (DGC-PDE), is crucial in control of UPP production and surface attachment. DcpA is regulated by PruR, a protein with distant similarity to enzymatic domains known to coordinate the molybdopterin cofactor (MoCo). Pterins are bicyclic nitrogen-rich compounds, several of which are formed via a non-essential branch of the folate biosynthesis pathway, distinct from MoCo. The pterin-binding protein PruR controls DcpA activity, fostering cdGMP breakdown and dampening its synthesis. Pterins are excreted and we report here that PruR associates with these metabolites in the periplasm, promoting interaction with the DcpA periplasmic domain. The pteridine reductase PruA, which reduces specific dihydro-pterin molecules to their tetrahydro forms, imparts control over DcpA activity through PruR. Tetrahydromonapterin preferentially associates with PruR relative to other related pterins, and the PruR-DcpA interaction is decreased in a *pruA* mutant. PruR and DcpA are encoded in an operon that is conserved amongst multiple Proteobacteria including mammalian pathogens. Crystal structures reveal that PruR and several orthologs adopt a conserved fold, with a pterin-specific binding cleft that coordinates the bicyclic pterin ring. These findings define a new pterin-responsive regulatory mechanism that controls biofilm formation and related cdGMP-dependent phenotypes in *A. tumefaciens* and is found in multiple additional bacterial pathogens.

24 **SIGNIFICANCE**

25 Biofilms are bacterial communities attached to surfaces, physiologically distinct
26 from free-living cells, and a common cause of persistent infections. Here we define the
27 mechanism of a novel biofilm regulatory system based on excreted metabolites called
28 pterins, that is conserved within a wide range of Gram-negative bacteria, including
29 multiple pathogens of animals and plants. The molecular mechanism of pterin-
30 dependent regulation is reported including structural determination of several members
31 of a new family of pterin-binding proteins. Pterins are produced across all domains of
32 life and mechanistic insights into this regulatory circuit could lead to new advances in
33 antibiofilm treatments.

34

35 **INTRODUCTION**

36 The regulation of bacterial attachment to surfaces plays a critical role in the formation of
37 biofilms and can dictate their maturation. Biofilms are surface-associated microbial
38 assemblages that are common among bacteria, and result in dramatic physiological
39 changes including substantial tolerance towards antibiotic treatment (1, 2). Biofilms
40 represent a major challenge for the treatment of bacterial infections as these
41 multicellular structures are recalcitrant to standard therapies and act as protective
42 reservoirs for pathogenic bacteria. Production of bacterial surface structures known as
43 adhesins drive stable attachment of bacteria to surfaces, the first step in biofilm
44 formation (3). Regulation of adhesin elaboration and activity thus can influence where
45 and how biofilm formation occurs. In many bacteria the transition from a free-living to a
46 sessile mode of growth is under the regulatory control of the cytoplasmic second
47 messenger cyclic diguanylate monophosphate (cdGMP). Increasing levels of cdGMP
48 often promote attachment and biofilm formation through production of adhesive proteins
49 and polysaccharides that drive the attachment process (4). Synthesis of cdGMP is
50 catalyzed by diguanylate cyclases (DGCs) and its turnover is driven by
51 phosphodiesterases (PDEs). Single bacterial taxa can have multiple DGCs and PDEs
52 that influence the cdGMP pool, and multi-domain proteins with dual DGC and PDE
53 activities are not uncommon. Environmentally responsive modulation of cdGMP pools is
54 mediated through control of gene expression and through allosteric regulation of these
55 enzymes, many of which have sensory input modules. The flux of this second
56 messenger in cells reflects the combined output of these synthesis and degradation
57 activities (5).

58 The facultative plant pathogen, *Agrobacterium tumefaciens*, utilizes secreted
59 polysaccharides to stably attach to biotic and abiotic surfaces, most prominently
60 cellulose and a polar adhesin known as the unipolar polysaccharide (UPP) (6). *A.*
61 *tumefaciens* is the causative agent of crown gall, a plant neoplastic disease that results
62 from bacteria-to-plant horizontal gene transfer (7). Attaching to plant tissue is a requisite
63 step in the virulence pathway of *A. tumefaciens*, but pathogenesis also involves
64 additional plant-produced-signals to activate virulence (8). Production of the UPP, as
65 well as cellulose, is under complex environmental control through cdGMP (9, 10). *A.*
66 *tumefaciens* encodes close to 30 proteins with predicted DGC domains and only two
67 solo PDE enzymes, but multiple proteins with predicted DGC domains also have PDE
68 domains (6).
69 In our prior studies, we identified the DcpA protein, with both canonical DGC and
70 PDE domains (9). DcpA has DGC and PDE activity *in vivo*, and genetic evidence
71 suggests that both domains are functional. However, under standard laboratory
72 conditions, DcpA is predominantly a PDE, maintaining low cdGMP levels and thereby
73 limiting surface attachment. The N-terminal portion of DcpA has two transmembrane
74 domains that flank an ~140 aa periplasmic domain of unknown function. Our prior
75 findings identified several other regulatory components critical for maintaining DcpA as
76 a PDE. These additional regulators include the PruA pteridine reductase, which reduces
77 specific 7,8-dihydropterins to their 5,6,7,8-tetrahydro forms, and PruR, a putative pterin-
78 binding protein (9, 11). Both of these proteins are required to regulate the enzymatic
79 activity of DcpA, and null mutants for *pruA* and *pruR* similarly lead to elevated cdGMP
80 and aberrant activation of surface adhesion. The *pruR* gene is transcriptionally coupled

81 with *dcpA* in a two gene operon, consistent with their related functions.

82 Pterins are characterized by a nitrogen-rich, bicyclic ring structure with side
83 chains of varying length and modifications extending from the ring carbon at the sixth
84 position (12). Well known biomolecules with a pterin ring include the folates in which the
85 side chain is composed of a para-amino benzoic acid group conjugated to a glutamic
86 acid residue (or poly-glutamate). Folate derivatives are required as cofactors for multiple
87 aspects of one-carbon metabolism, and folate is essential in most organisms (13). More
88 broadly, diverse pterin derivatives are found in all domains of life, and in bacteria are
89 known to act as enzymatic cofactors. Molybdopterin cofactor (MoCo) is a complex
90 molybdenum-containing derivative used by various organisms as a prosthetic group to
91 catalyze redox reactions. MoCo is synthesized from GTP via a pathway independent
92 from folate biosynthesis (14). Biopterin and monapterin are pterins with hydroxylated 3
93 carbon side chains that function with cytoplasmic amino acid hydroxylases, but
94 curiously the dominant fraction of pterins is detected outside of cells (15). Pterins can
95 exist in a fully oxidized state as well as the reduced 7,8-dihydro and 5,6,7,8-tetrahydro
96 states, the latter of which serves as the biologically active form of the respective
97 cofactor. In *A. tumefaciens,* PruA catalyzes the NADPH-dependent reduction of H_2MPt
98 to H_4MPt (11). Extracts of *A. tumefaciens* contain a methylated derivative of H_4MPt (2′-
99 *O*-methylmonapterin) but this is undetectable in *pruA* deletion mutants and in mutants
100 expressing a catalytically inactive PruA protein (9). Mutations that interfere with PruA
101 activity result in high level DGC activity from DcpA, driving elevated UPP-dependent
102 adhesion.

103 The regulation of DcpA by PruA is indirect and requires PruR, but the

104 mechanistic basis for this was undefined (9)(Fig. S1A). PruR shares distant amino acid
105 sequence similarity with the SUOX family of proteins, defined by sulfite oxidases and
106 related enzymes, including YedY from *Escherichia coli* (16). SUOX proteins have
107 domains that associate with MoCo to facilitate their enzymatic activities and have a
108 conserved cysteine residue that coordinates the molybdenum atom in MoCo. There is
109 no cysteine at this position in PruR and the protein has no predicted enzymatic activity
110 (9, 17). Rather, we hypothesize that PruR is a pterin-binding protein functioning with
111 non-MoCo pterin derivatives. Here we report on the pterin-response mechanism, the
112 structure of PruR, its control of DcpA, and conservation of this system in multiple
113 bacterial pathogens.
114

115 **RESULTS**

116 **PruR regulates DcpA and binds to pterin ligands *in vitro***

117 The impact of elevated cdGMP on UPP and cellulose production can be
118 qualitatively observed by cultivating *A. tumefaciens* derivatives on solid medium
119 supplemented with the azo-dye Congo Red – increased red pigmentation of colonies
120 (the elevated Congo Red or ECR phenotype) is indicative of increased polysaccharide
121 production (10). The ECR phenotype is also predictive for increased surface adhesion
122 via the UPP. The *pruR* gene (ATU_RS16195) is encoded in an operon 9 bp immediately
123 upstream of *dcpA* (ATU_RS16200). Our previous studies revealed that a precise in-
124 frame deletion of the entire *pruR* coding sequence leads to a *dcpA*-dependent ECR
125 phenotype and increased biofilm formation via elevated UPP production (9). We
126 constructed a new deletion mutant, preserving potential translational coupling with

127 *dcpA*, while deleting most of the *pruR* gene. This new Δ*pruR* mutant exhibited a
128 pronounced ECR phenotype and increased biofilm formation, and in contrast to our
129 prior Δ*pruR* mutant, which impacted downstream *dcpA* expression (9), was well
130 complemented with ectopic expression of *pruR* alone (Fig. S1B, S1C).
131 PruR was purified from *E. coli* to examine pterin binding *in vitro*. A restricted set
132 of pterins are available commercially, and the tetrahydro forms are quite susceptible to
133 oxidation. We synthesized an optically active H_2MPt from L-xylose by following a related
134 reported procedure (18) and obtained dihydroneopterin (H_2NPt), dihydrofolate (H_2F) and
135 tetrahydrofolate (H_4F) from commercial sources. Our prior studies established that the
136 *A. tumefaciens* pteridine reductase PruA reduces H_2MPt and H_2NPt (11). An enzyme-
137 coupled binding assay was developed to actively convert the dihydropterins to their
138 tetrahydro derivatives (Fig. 1A), in which purified pteridine reductase PruA (His_6-PruA)
139 was incubated with the dihydropterin substrates and NADPH and in the presence of
140 purified non-tagged PruR under anaerobic conditions. Extracted pterins bound to PruR
141 were oxidized and measured by HPLC separation by fluorescence measurement (folate
142 was detected by UV) (Fig. S2). PruR associated with H_2MPt at detectable levels but
143 bound considerably more of the pterin in the PruA-coupled reaction, indicating
144 increased affinity for the fully reduced H_4MPt (Fig. 1B p-value <0.05 compared to all
145 other pterins). PruR also weakly associated with the neopterin derivatives but did not
146 show a statistically significant preference for H_4NPt compared to H_2NPt. PruR bound
147 even less well to H_2F, with no preference for H_4F; both folate compounds were bound
148 significantly less well than H_4MPt and H_4NPt.
149

150 **PruR actively modulates the DGC and PDE activity of DcpA**

151 The *in vivo* phenotypes of several *dcpA* point mutants suggested that it has both
152 DGC and PDE activity, but that the PDE activity is dominant in planktonic laboratory
153 culture (9, 10). Enzymatic assays of the purified DcpA cytoplasmic domain (res. 190-
154 644, see Methods) revealed that the protein has both activities (Fig. S3), although the
155 DGC activity is weaker (0.26 A_{360} units $min^{-1}mol^{-1}$) compared to PDE activity (15.7 A_{360}
156 units min^{-1} mol^{-1}). However, it was unclear whether the PruR-dependent PDE-dominant
157 activity of DcpA *in vivo* reflects PruR stimulation of the PDE activity, the inhibition of
158 DGC activity, or both.

159 Ectopic expression of *dcpA* alone in *E. coli*, in the absence of *pruR*, resulted in
160 high level cdGMP synthesis and mutation of the DGC catalytic motif (GGDEF>GGDAF;
161 E308A) abolished this cdGMP increase, suggesting that PruR is required for dominant
162 PDE activity (9). Plasmid-borne expression of wild type *dcpA* complements the elevated
163 biofilm formation of *the* Δ*dcpA* mutant to normal levels. By contrast, the Δ*pruR*Δ*dcpA*
164 mutant harboring this plasmid exhibits a dramatic increase in biofilm formation relative
165 to wild type, and higher than the single *dcpA* mutant (Fig. 1C), consistent with the
166 increased cdGMP caused by *dcpA* ectopic expression in a *pruR* null mutant (9).
167 Expression of the $DGC^-(PDE^+)$ $DcpA_{E308A}$ allele in the Δ*dcpA* mutant decreases biofilm
168 formation to wild type levels. However, this allele fails to cause this decrease in the
169 Δ*pruR*Δ*dcpA* mutant, suggesting that PDE activity is under PruR control. Ectopic
170 expression of *dcpA* in wild type does not significantly diminish biofilm formation (likely
171 due to cdGMP production by other DGCs) (9).

172 In the absence of PruR, the PDE activity of DcpA is not increased by ectopic

173 expression of DcpA. Mutation of *dcpA* to abolish DcpA PDE activity (EAL>EEL; E431A;
174 $PDE^{-}DGC^{+}$) resulted in striking stimulation of biofilm formation when this mutant is
175 ectopically expressed in the Δ*dcpA* mutant (Fig. 1C). However, expression of the
176 $DcpA_{E431A}$ allele in the Δ*pruR*Δ*dcpA* mutant imparts even more dramatic biofilm
177 stimulation, suggesting that PruR dampens DGC activity in addition to stimulating PDE
178 activity, and its effects on these two activities are genetically separable. Ectopically
179 expressing an allele mutated for both domains ($DGC^{-}PDE^{-}$, E308A E431A,) does not
180 strongly impact biofilm formation in either the Δ*dcpA* or the Δ*pruR*Δ*dcpA* mutant but
181 shows a slight increase in the *pruR-dcpA* double mutant relative to the Δ*dcpA* mutant.
182

183 **PruR is secreted and active in the periplasm**

184 Sequence analysis suggests that the PruR protein has an N-terminal secretion
185 signal (aa 1-22, Signal-P score 0.31, Fig. 2A). Given our hypothesis that PruR is a
186 pterin-binding protein, this prediction is surprising, as the only established function of
187 bacterial pterins is to serve as cofactors for amino acid hydroxylases, which are
188 cytoplasmic enzymes (15). To experimentally evaluate whether PruR is secreted to the
189 periplasm *in vivo*, we first tested this genetically by fusing it to *phoA*, encoding the
190 enzyme alkaline phosphatase (AP) that requires localization to the periplasm for activity
191 (19). Plasmid-borne, ectopic expression of the *pruR-phoA* fusion in *A. tumefaciens* led
192 to detectable AP activity in whole cells, above the very low levels of the same strain with
193 no *phoA* (Fig. S4A). Furthermore, fusion of only the *pruR* signal sequence (res. 1-22)
194 with *phoA* ($pruR_{SS}$-*phoA*) similarly expressed from the same plasmid resulted in much
195 stronger AP activity. Neither construct was affected by expression in the Δ*pruR* null

196 mutant. It is likely that the full length PruR-PhoA fusion partially diminishes AP activity.

197 The periplasmic localization of PruR was tested directly by fractionating *A.*
198 *tumefaciens* cells from wild type and several derivatives into periplasmic and
199 cytoplasmic fractions using an osmotic shock protocol and probing western blots with a
200 polyclonal antibody preparation raised against PruR (α–PruR). Wild type cells clearly
201 revealed a protein the size of the processed from of PruR (146 aa, predicted 16.1 kDa)
202 in the periplasmic fraction, whereas a Δ*pruR* mutant lacked this protein (Fig. 2B).
203 Ectopic expression of a plasmid-borne copy of *pruR* expressed from P_{lac} in the Δ*pruR*
204 mutant revealed an IPTG-inducible PruR protein in the periplasmic fraction. In contrast
205 the same expression construct deleted for the *pruR* signal sequence (Δ_{SS}*pruR*) results
206 in PruR that remains in the cytoplasmic fraction.

207 Complementation of a Δ*pruR* mutant (the mutation which is partially polar on
208 *dcpA*) with a plasmid expressing *pruR* and *dcpA* rescues this mutant to normal levels of
209 surface attachment (Fig. 2C). However, expression of the same plasmid expressing the
210 Δ_{ss}*pruR* allele and *dcpA* failed to rescue these phenotypes (Fig. 2C). The even greater
211 surface adherence observed with the (P_{lac}-Δ_{ss}*pruR-dcpA*) plasmid was most likely due
212 to its additional copy of *dcpA*.

213 Although PruR has a match for an N-terminal signal sequence there was an even
214 stronger match identified for a lipidation site in the signal sequence predicted at the
215 cysteine 19 (C19, Signal-P score 0.68, Fig. 2A) (20). In this analysis, PruR would be
216 lipidated at C19 with signal peptidase cleavage between it and the adjacent serine (S18,
217 Fig. 2A), rather than A22 as predicted for the non-lipidated secretion signal. Lipidated
218 PruR would be predicted to associate with the periplasmic leaflet of the inner membrane

219 rather than the outer membrane (21). Although this predicted lipidation site is an
220 imperfect match to the spacing for the canonical sequence “lipobox” motif
221 (L[A/S][A/G]C), we tested whether C19 is required for PruR activity. Ectopic expression
222 of a *pruR* allele with this cysteine residue mutated to an alanine (C19A) fully
223 complemented the elevated biofilm phenotype Δ*pruR* mutant, suggesting that PruR is
224 not lipidated, or minimally that it does not have to be anchored to the inner membrane to
225 function in the periplasm (Fig. S4B). Furthermore, *pruR* was effectively secreted and
226 retained full activity when fused with the *malE* and *dsbA* signal sequences ($MalE_{SS}$ and
227 $DsbA_{SS}$) from *E. coli*, well characterized to direct two distinct Sec-dependent secretion
228 mechanisms, and to be non-lipidated (22, 23) (Fig. S4C and S4D).
229
230 ***In vivo* crosslinking reveals a PruR-DcpA complex**
231 Direct interaction of PruR with the periplasmic region of DcpA would be one
232 mechanism by which pterins could regulate DcpA DGC and PDE activity. To test this
233 hypothesis, we used disuccinimidyl suberate (DSS) to perform protein crosslinking with
234 cell suspensions of *A. tumefaciens* and then probed for PruR and DcpA proteins using
235 polyclonal antibodies to PruR and separately to the periplasmic portion of DcpA (Fig. 3).
236 PruR is an approximately 16 kDa protein, and full-length DcpA is approximately 70 kDa.
237 Upon DSS addition in wild type cells, SDS-PAGE separation, and western blotting with
238 α-PruR antibody, a new protein species of ~85 kDa is observed (Fig. 3A). This species
239 is absent in the Δ*dcpA* mutant but is significantly more pronounced in wild type *A.*
240 *tumefaciens* expressing the P_{lac}-*pruR-dcpA* construct. Elevated expression of the *pruA*
241 gene had no obvious impact on crosslinking of PruR and DcpA. Probing these western

242 blots with a lower titer α-DcpA antibody preparation against the periplasmic domain
243 captured the complex in cells harboring the P_{lac}-*pruR-dcpA* plasmid but was not
244 sufficiently sensitive to detect the complex at native levels of expression (Fig. S5).
245 Next, we tested the interaction of PruR independently with the periplasmic and
246 cytoplasmic DcpA domains. The DcpA periplasmic domain including its two
247 transmembrane elements (expressing codons 1-192) and the DcpA cytoplasmic
248 expression plasmid (codons 190-644) were independently expressed from P_{lac} either in
249 the wild type or the Δ*dcpA* mutant. DSS crosslinking of whole cell suspensions revealed
250 efficient PruR crosslinking with the DcpA periplasmic domain (predicted ~37.4 kDa
251 crosslinked complex) but not with the cytoplasmic domain (predicted 66.5 kDa complex)
252 (Fig. 3B). In the wild type background, the full length PruR-DcpA complex was also
253 visible, when probed for either PruR or the periplasmic domain of DcpA, but this was
254 abolished in the Δ*dcpA* mutant. These results are consistent with the genetic evidence
255 that the PruR-DcpA interaction occurs in the periplasm.
256
257 **PruR interaction with the DcpA periplasmic domain is decreased in a *pruA* mutant**
258 The Δ*pruA* mutant manifests a dramatic increase in UPP production and surface
259 attachment, similar to mutants of *pruR* or *dcpA*, and its impact is dependent on the
260 presence of a functional *dcpA* gene (9). To evaluate whether PruA-generated H_4MPt
261 impacts PruR-DcpA interactions, we compared DSS crosslinking for whole cell
262 suspensions of the Δ*pruA* mutant compared to the wild type, both ectopically expressing
263 PruR and the periplasmic domain of DcpA (these derivatives retain the chromosomal
264 *pruR-dcpA* genes). The amount of complex formation between PruR and $DcpA_{Peri}$ was

265 substantially diminished in the Δ*pruA* mutant relative to the wild type using both the
266 α–PruR (Fig. 4A) and α–DcpA$_{Peri}$ (Fig. 4B) antibodies. These results suggest that *pruA*
267 is required for maximal complex formation between PruR and DcpA and suggests that
268 pterins formed by PruA are essential for the PruR and DcpA interaction.
269
270 **Conservation of *pruR-dcpA* type operons among proteobacterial pathogens**
271 We next sought to determine whether PruR is conserved in other bacteria. There
272 are well-conserved homologs of PruR in several taxa within the Alpha- and Gamma-
273 proteobacteria (Fig. 5). All of these proteins are of similar sizes with an N-terminal
274 secretion signal and share residues common among the SUOX family of proteins (see
275 residues marked by asterisks in Fig. S6A). Notably, all lack the critical cysteine involved
276 in MoCo binding in SUOX proteins, and instead have a tryptophan. None of these has a
277 Cys in their N-terminal signal sequence consistent with our finding that this residue is
278 dispensable for PruR function (Fig. S6A). Additionally, inspection of the genomic
279 location for the PruR homologs in these proteobacteria reveal presumptive bicistronic
280 operons with a downstream gene encoding a DcpA homolog which is comprised of two
281 transmembrane domains flanking a periplasmic loop and a large cytoplasmic portion of
282 the protein. Many of these have both DGC and PDE domains such as DcpA, although in
283 some cases they have only the DGC domain without the C-terminal PDE (Fig. 5). The
284 predicted periplasmic domains of these *dcpA* homologs are roughly the same length
285 (138-150 aa) and are chemically similar. However, these regions are only weakly
286 conserved at the primary amino acid sequence level, with two invariant residues in
287 common, a tryptophan and a glutamate (W40 and E48 in the full-length *A. tumefaciens*

288 DcpA) (Fig. S6B). Strikingly, most of the bacteria that encode this *pruR-dcpA* operon
289 are opportunistic pathogens of animals or plants. Interestingly, *Vibrio cholerae* has two
290 *pruR-dcpA* operons, VC1933-1934 and VCA0075-0074 (Fig. 5). The VC1934 DcpA
291 homolog has both DGC and PDE domains, but the GGDEF motif is degenerate
292 (GADEF) and likely inactive. Conversely, the VCA0074 DcpA homolog only has the
293 GGDEF domain without the PDE domain. In fact, VCA0074 is the well-studied CdgA
294 protein established to have DGC activity in *V. cholerae* and to play an important role in
295 biofilm formation (24).
296
297 **PruR-type proteins share a common structural fold**
298 Based on our experimental findings for PruR-pterin interactions and on sequence
299 conservation, we hypothesized that PruR represents a new class of proteins with an
300 overall fold similar to the MoCo binding domains of SUOX-type proteins, that instead
301 bind to the non-MoCo pterins. We purified representative members of the PruR family
302 and determined their three-dimensional structures by X-ray crystallography (Table S2).
303 The *A. tumefaciens* PruR structure reveals a general structural motif comprised of 10 β-
304 sheets and 7 α-helices (Fig. 7A, PDB 7kou). The β-strands form one mixed, five-
305 stranded β sheet (2-1-10-5-6) and one curved, four-stranded antiparallel β sheet (3-4-7-
306 9), and these sheets are interconnected by short α helices (1, 2, 3, 5, 6 and 7). We
307 solved an additional crystal structure of *A. tumefaciens* PruR (PDB 7kos) for which the
308 overall structure is identical except that in this crystal form a small surface pocket is
309 occupied by the side chain residues of neighboring or symmetry related polypeptide
310 chains (Fig. S7 and Table S1).

311 Structures of three other PruR homologs were also solved including proteins
312 from *V. vulnificus* (PDB 7kom, 30% identity; 1 Å), *V. cholerae* (PDB 7kp2, 32% identity,
313 1.03 Å), and *K. pneumoniae* (PDB 7rkb, 59% identity, 2.5 Å) (Fig. 6B and 6C). Multiple
314 sequence and structure alignments of these PruR homologs clearly show that the
315 structures are highly similar (root-mean-squared-deviation (RMSD) of 0.6 – 2.0 Å) and
316 all share the SUOX-like fold. Overall, the PruR fold is conserved in different Alpha- and
317 Gammaproteobacteria, consistent with a similar function for PruR in these bacteria.
318
319 **PruR has a shortened MoCo binding site that associates with a pterin**
320 Structural comparison of *A. tumefaciens* PruR to chicken liver sulfite oxidase
321 (PDB 1sox), a relatively close SUOX structural homolog, and *E. coli* YedY (PDB 1xdq),
322 a more distant sequence homolog, revealed significant structural overlap to the MoCo
323 binding domains (Fig. 7A and 7B). PruR from *A. tumefaciens* aligns over 126 aa
324 residues with the chicken liver SUOX protein with an RMSD value of 2.5 Å. The chicken
325 liver SUOX active site contains a single molybdopterin bound to a surface cleft
326 characterized by the conserved cysteine residue at the end of a lengthy β-hairpin (Fig.
327 7A). There is no surface cleft that could accommodate MoCo in the equivalent region of
328 PruR, and the β-hairpin with the conserved Cys residue in all SUOX proteins, including
329 in *E. coli* YedY (res. 138-146; (25), is truncated in PruR (res. 161-166). Furthermore,
330 structural-sequence alignments of PruR, YedY, and chicken liver sulfite oxidase show
331 that the canonical molybdenum-coordinating cysteine is substituted with a tryptophan
332 (W70) in PruR, which constitutes a proline-tryptophan (^{69}PW^{70}) motif conserved in PruR
333 homologs (Fig. 6C). Thus, the PruR fold is like that of SUOX family MoCo-binding

334 domains but several structural determinants for MoCo binding, including a deep binding
335 cleft, are lacking. The smaller pocket identified in our structures, however, can
336 accommodate a smaller non-MoCo pterin molecule.

337 To examine the pterin-PruR interaction, we co-crystallized PruR with H_2NPt, a
338 commercially available monapterin stereoisomer that is more stable to oxidation than
339 the tetrahydro pterins and thus compatible with crystallization methods. We obtained the
340 ligand-bound structures for both *K. pneumoniae* and *V. cholerae* PruR homologs (7rkb
341 and 7kp2, respectively) (Fig. 7C). Refinement revealed both were bound by the bicyclic
342 moiety of the neopterin, with the hydroxylated tail absent. In all structures, the neopterin
343 ring is positioned in the pterin binding cleft and is sandwiched between a tyrosine and
344 tryptophan (*A. tumefaciens* Y104 and W160, respectively) (Fig. 7C). The pterin also
345 forms hydrogen bonds with an asparagine residue (N102). These three residues are
346 conserved across all PruR homologs (Fig. 6C), and Y104 is conserved in other SUOX
347 proteins including YedY (Fig. 7B). Notably, in our apo structure of *A. tumefaciens* PruR,
348 the Y104 side chain is flipped away from the pterin binding pocket (Fig. 7C), suggesting
349 that binding of a ligand to this cleft induces key stacking interactions that stabilize the
350 pterin in the site. Further comparison of the pterin-bound PruR structures also revealed
351 three alternative binding conformations of neopterin. The orientation of the ring moiety
352 varies, yielding different positions of the hydroxylated tail (Fig. 7D and Fig. S8A-C). We
353 suspect that the observed variation in binding modes of neopterin is a result of
354 differences between this disfavored fully oxidized ligand and the cognate reduced
355 H_4MPt and/or 2′-*O*-Met-H_4MPt (9).
356

357 **DISCUSSION**

358 Here we describe the regulation of the dual-function DGC/PDE DcpA by a novel
359 pterin-binding protein PruR, building from our previous findings (9-11). All three
360 components of the pterin regulatory pathway discussed here (PruR, DcpA, and PruA)
361 were identified in a transposon mutagenesis screen designed to identify novel
362 regulators of surface attachment in *A. tumefaciens* (10). In this study we have further
363 interrogated this pterin regulatory pathway by (i) characterizing how the pterin-binding
364 protein PruR regulates DcpA activity, (ii) defining PruR as a periplasmic protein that
365 interacts with DcpA as well as H_4MPt, (iii) elucidating the role of PruA in promoting the
366 interaction between PruR and DcpA, and (iv) identifying similar regulatory systems in
367 other *Proteobacteria*. Furthermore, we determined the three-dimensional structure of
368 PruR and selected homologs in their apo forms, and two as a complex with a pterin.
369 The level of conservation of PruR and DcpA homologs among multiple *Proteobacteria*
370 suggests that they are likely to also utilize pterin-dependent regulation of cdGMP pools.
371

372 **A new class of pterin binding proteins**

373 Our findings suggest that PruR and its homologs are a new type of pterin-binding
374 periplasmic protein and we report the first structural information for this new group. The
375 overall fold of PruR-type proteins suggests that they are a branch of the SUOX protein
376 family, cytoplasmic enzymes including sulfite oxidases and nitrate reductases that utilize
377 MoCo as a co-factor (16). Most SUOX proteins are large and have additional domains
378 that drive catalysis. In contrast PruR-like proteins are small, almost entirely comprised
379 of the SUOX fold and their N-terminal secretion signal. Pterins such as H_4MPt and

380 related molecules are significantly smaller and less structurally complex than MoCo. It is
381 intriguing that the pterin binding site for PruR-type proteins and the SUOX MoCo
382 binding site are structurally and likely evolutionarily related, especially given the
383 markedly different functions of the two groups of proteins.

384 Other proteins known to bind the bicyclic pteridine ring are the aromatic amino
385 acid hydroxylases such as phenylalanine hydroxylase (PAH), which coordinates a
386 tetrahydrobiopterin (H_4BPt) molecule as a cofactor. The H_4BPt binding site stabilizes the
387 pteridine ring via a conserved acidic residue and a histidine-conjugated iron atom, which
388 interact with ring positions 2 and 4, respectively (26). This binding site thus bears no
389 significant similarity to the SUOX-type pterin binding site of the PruR-type proteins we
390 define here. There are also well studied, membrane-anchored mammalian proteins that
391 associate with the essential metabolite tetrahydrofolate (H_4F), which also contains the
392 bicyclic pteridine ring. These folate binding proteins (FBPs) are upregulated in fetal cells
393 and certain cancers (27, 28), and dramatically alter their conformation upon binding to
394 H_4F. Similar to PruR-like proteins, their association with the pteridine ring in H_4F is
395 fostered by conserved Tyr and Trp residues that sandwich the ring in a hydrophobic
396 pocket, although these proteins are otherwise structurally distinct the PruR-type proteins
397 reported here.

398

399 **Preference of PruR for fully reduced monapterin**

400 The pterin binding specificity of PruR was revealed by *in vitro* studies with
401 purified PruR and different pterin species. Fully reduced tetrahydropterins oxidize
402 readily to the dihydropterin forms (29). We used a coupled enzyme reaction with the

403 PruA pteridine reductase and NADPH in the presence of H_2MPt and H_2NPt under
404 anoxic conditions to generate the respective tetrahydropterin species in the presence of
405 PruR (11). We observed significantly greater association of the monapterin species in
406 the presence of PruA than in its absence, consistent with greater binding to the PruA-
407 generated H_4MPt. In contrast, neopterin binding to PruR was lower and unaffected by
408 the presence of PruA, even though our prior *in vitro* PruA work revealed similar catalytic
409 efficiency with H_2MPt and H_2NPt substrates (11). PruR detectably binds the neopterin
410 species and the reduced folate species, but not to the same extent as the PruA-
411 generated H_4MPt. Although this experiment is evidence for the pterin association with
412 PruR, it does not provide binding affinities.

413 Co-crystallization with the H_2NPt ligand and the PruR homologs from *V. cholerae*
414 (7KOU) and *K. pneumoniae* (7RKB) revealed the fully oxidized neopterin (presumably
415 due to oxidation of the exogenously added H_2NPt during crystallization) binding at the
416 analogous location as the MoCo binding site on SUOX. Pterin binding occurs within the
417 pterin-binding cleft we have defined on the PruR-type proteins through interaction of the
418 pteridine ring sandwiched between the conserved Tyr and Trp residues and several
419 other hydrogen bonding positions. The hydroxylated tail of the neopterin was not visible
420 in these structures suggesting greater mobility. The stereochemistry of the hydroxylated
421 tail distinguishes monapterin from its stereoisomer neopterin, and the more complex
422 benzoyl and glutamyl side chain substituents of folate, and we hypothesize that
423 interactions between this tail and PruR add binding specificity. Additionally, the binding
424 site may also interact directly with the fully reduced tetrahydropterin species through
425 interactions that are not observed in the crystal structures with oxidized neopterin. The

426 multiple positions of the neopterin detected within the binding cleft may also reflect
427 weaker interactions of the protein with the non-cognate, fully oxidized neopterin
428 molecule.
429
430 **PruR interacts with pterins in the periplasm**
431 PruR negatively regulates surface attachment in *A. tumefaciens* through
432 modulation of DcpA activity. Loss of function mutations in the pteridine reductase gene
433 *pruA*, preventing H_4MPt synthesis largely phenocopy *pruR* null mutants. The best
434 studied functions for bacterial pterins are to act as enzymatic cofactors for amino acid
435 hydroxylase enzymes such as phenylalanine hydroxylase (15). All evidence suggests
436 that PruA drives reduction of H_2MPt in the cytoplasm, but our findings have revealed
437 that PruR functions and responds to pterins in the periplasm. A longstanding,
438 unexplained observation among reports on bacterial pterins is that they accumulate
439 extracellularly, with as much as 100-fold greater pterin in the extracellular fraction as
440 compared to associated with cells (15, 30). The mechanism of excretion has not been
441 elucidated, but it is also thought that extracellular pterins can re-enter cells (31). The
442 PruR protein clearly interacts with a self-produced, reduced monapterin species in the
443 periplasm, but exogenous pterins that enter the periplasm might also act as agonists or
444 antagonists of the H_4MPt-PruR interaction. Our findings are most consistent with H_4MPt
445 preferentially binding to PruR. However, H_4MPt is susceptible to oxidation and thus will
446 have a relatively short half-life in the periplasm and elsewhere outside the cell (32).
447
448

449 **Interaction of PruR and DcpA is stimulated by PruA**

450 Crosslinking in whole cells reveals that PruR and DcpA interact through the DcpA
451 periplasmic domain to form a stable complex. The size of the crosslinked species (~85
452 kDa) suggests that the proteins are in a one-to-one stoichiometry. The crosslinked
453 product between ectopically expressed PruR and the DcpA periplasmic domain is
454 significantly diminished in the Δ*pruA* mutant, although it is still detectable. The Δ*pruA*
455 mutant has a dramatic phenotype in which DcpA exhibits predominantly DGC activity,
456 equivalent to the Δ*pruR* mutant (9), so whatever remaining interaction occurs between
457 the two proteins is insufficient to maintain a strong DcpA PDE bias. Our analysis of the
458 PruR control of DcpA catalytic site mutants suggests that in cells with active PruA, the
459 PruR-DcpA interaction stimulates PDE activity and also diminishes DGC activity. We
460 speculate this may be due the reciprocal control of dimerization for the separate DGC
461 and PDE domains of DcpA, known to be required for these activities in other proteins
462 that synthesize and degrade cdGMP (33, 34).

463 The DcpA periplasmic domain is less well conserved among the DcpA orthologs,
464 although there are two invariant residues, Trp40 and Glu48 (in *A. tumefaciens* DcpA).
465 The domains are all roughly 140 aa in length with dispersed chemical conservation.
466 Alpha Fold predictions suggests that the DcpA periplasmic domain forms a novel four
467 helix CACHE-type bundle, with overall structural similarity to the four helix bundles in
468 the periplasmic domains of methyl-accepting dependent chemotaxis proteins (MCPs),
469 that impart chemotactic motility responses to certain solutes (35). Rather than
470 interacting directly with their ligands in the periplasm, several MCPs mediate the
471 response through interactions with periplasmic solute binding proteins (SBPs) (36). The

472 interaction of PruR and the DcpA periplasmic domain may share similarities with MCP-
473 SBP interactions, with binding of the pterin fostering this interaction.
474 The PruR-DcpA system is strikingly analogous to the dual-function DGC-PDE
475 MbaA in *V. cholerae*, which is regulated through the interaction of its periplasmic
476 domain with NspS (37, 38). NspS is a SBP for polyamines and is encoded upstream of
477 *mbaA* in the same operon. The specific type of polyamine bound by NspS can regulate
478 its interaction with MbaA, thereby controlling the balance of DGC and PDE activities
479 from this enzyme. *V. cholerae* synthesizes and releases norspermidine, which
480 stimulates DGC activity through NspS-MbaA interactions, whereas other polyamines
481 such as spermidine inhibit association with MbaA. (39, 40). The polyamine response
482 impacts cdGMP levels, controlling *V. cholerae* biofilm formation. Interestingly, in the
483 absence of polyamines, NspS can bind to MbaA and weakly impacts its activity, similar
484 to our observation here that PruR weakly binds to DcpA in the absence of its proposed
485 H_4MPt ligand. There are multiple types of pterins produced and excreted by bacterial
486 and eukaryotic organisms (12), and it is conceivable that similar to the NspS-MbaA
487 system, the specific pterin-associated with PruR can impact its regulation of DcpA.
488 These structurally variant pterins may act as agonists or antagonists for the PruR-H_4MPt
489 interaction. It is also plausible that the PruR-associated pterin acts as a proxy to detect
490 a different cue in the periplasm, such as specific redox-active compounds.
491
492 **Insights into conserved PruR-DcpA type systems in other bacteria**
493 The PruR homologs we identify here are well conserved proteins and highly likely
494 to be orthologous in function. The structural determination of the four different PruR-

495 type apo-proteins all had high similarity with an RMSD value of <2.0 Å. This similarity
496 includes the residues we have identified that associate with the pteridine ring. Most of
497 these *pruR* homologs are immediately upstream of *dcpA* homologs with both the DGC
498 and PDE domains similar to DcpA, or only the DGC domain. The periplasmic domains
499 of these DcpA-type proteins are of similar size and amino acid chemistry but with only
500 the two fully conserved residues mentioned above. For some of the conserved *pruR*-
501 *dcpA* operons, only one of the cdGMP functions is retained. For example, there are two
502 of these conserved operons in *V. cholerae*, VC1933-VC1934 and VCA0075-VCA0074
503 (VCA0074 is the well-studied DGC known as CdgA, (24)). Interestingly VC1934 is
504 unlikely to be active for cdGMP synthesis (due to its nonfunctional GADEF motif) but
505 active for its degradation, and CdgA is well established to be active for cdGMP
506 synthesis (24, 41). In combination they may provide similar, but independently regulated
507 DGC/PDE activities, as does the dual functionality of DcpA in *A. tumefaciens.* In the two
508 major model strains of *P. aeruginosa*, PA01 and PA14, mutants for their *dcpA* homologs
509 (PA2780/PA1426970), both impact cdGMP-dependent phenotypes, although to different
510 extents (42, 43). In all of these cases, the positioning of a *pruR*-type gene immediately
511 upstream is consistent with a regulatory relationship with the downstream gene. Given
512 the remarkable similarity of the PruR gene products, it is highly likely that they bind the
513 same or related pterin ligands and provide pterin-dependent control.
514
515

516 **MATERIALS AND METHODS**

517 Detailed descriptions of materials and methods can be found in the
518 Supplementary Information, including: bacterial strains and plasmids used (Tables S3
519 and S4), growth conditions, molecular cloning and site-directed mutagenesis, Congo
520 Red staining, biofilm formation quantification, PhoA secretion assays, antibody
521 production and purification, western blots, periplasmic fractionation, *in vivo* crosslinking,
522 HPLC analysis of pterins and folates, *in vitro* analysis of pterin binding to PruR, protein
523 crystallography (including molecular cloning, protein production and purification, data
524 collection, structure solution and refinement), purification of PruA, and *in vitro* enzymatic
525 assays for DcpA.

526

527 **DATA AVAILABILITY**

528 The structures determined here were deposited in the Protein Data Bank
529 (https://www.rcsb.org/) with the assigned PDB codes: 7kos (*A. tumefaciens*), 7kou (*A.*
530 *tumefaciens 2)*, 7kom (*V. vulnificus*), 7rkb (*K. pneumoniae*), 7kp2 (*V. cholerae*). Protein
531 diffraction data have been deposited at proteindiffraction.org. All additional experimental
532 data is available upon request from the authors.

533

534 **ACKNOWLEDGEMENTS**

535 We thank Fitnat Yildiz, Seth Rubin, Vanessa Mariscal, Thomas Bernhardt, and Jon
536 Beckwith for helpful discussions and Ramya Natarajan for technical assistance with
537 preliminary protein purification. This project was supported by grants to C.F. (NIH R01
538 GM120337), K.D.A (NSF-CHE 2105598), A.K.G. (AI150466.). N.F. received support

539 from the IU Genetics, Cellular and Molecular Sciences NIH Training Grant (T32
540 GM007757). Work by the Center for Structural Biology of Infectious Diseases was
541 supported by HHS/NIH/NIAID contracts #HHSN272201700060C and
542 75N93022C00035. This research used resources of the Advanced Photon Source, a
543 U.S. Department of Energy (DOE) Office of Science User Facility operated for the DOE
544 Office of Science by Argonne National Laboratory under Contract No. DE-AC02-
545 06CH11357. Use of the LS-CAT Sector 21 was supported by the Michigan Economic
546 Development Corporation and the Michigan Technology Tri-Corridor (Grant
547 085P1000817). Access to LS-CAT and computational resources is facilitated by the NU
548 Structural Biology Facility, which is supported by NCI grant to P30 CA060553 the
549 Robert H. Lurie Comprehensive Cancer Center.

550 **REFERENCES**

551 1. O. Ciofu, C. Moser, P. O. Jensen, N. Hoiby, Tolerance and resistance of
552 microbial biofilms. *Nat Rev Microbiol* **20**, 621-635 (2022).
553 2. K. Sauer *et al.*, The biofilm life cycle: expanding the conceptual model of biofilm
554 formation. *Nat Rev Microbiol* **20**, 608-620 (2022).
555 3. C. Berne, C. K. Ellison, A. Ducret, Y. V. Brun, Bacterial adhesion at the single-
556 cell level. *Nat Rev Microbiol* **16**, 616-627 (2018).
557 4. U. Jenal, A. Reinders, C. Lori, Cyclic di-GMP: second messenger extraordinaire.
558 *Nat Rev Microbiol* **15**, 271-284 (2017).
559 5. T. E. Randall *et al.*, Sensory perception in bacterial cyclic diguanylate signal
560 transduction. *J Bacteriol* **204**, e0043321 (2022).
561 6. M. A. Thompson, M. C. Onyeziri, C. Fuqua, Function and regulation of
562 *Agrobacterium tumefaciens* cell surface structures that promote attachment. *Curr*
563 *Top Microbiol Immunol* **418**, 143-184 (2018).
564 7. S. B. Gelvin, *Agrobacterium*-mediated plant transformation: the biology behind
565 the "gene-jockeying" tool. *Microbiol. Mol. Biol. Rev.* **67**, 16-37 (2003).
566 8. J. E. Heindl *et al.*, Mechanisms and regulation of surface interactions and biofilm
567 formation in *Agrobacterium*. *Frontiers in plant science* **5**, 176 (2014).
568 9. N. Feirer *et al.*, A pterin-dependent signaling pathway regulates a dual-function
569 diguanylate cyclase-phosphodiesterase controlling surface attachment in
570 *Agrobacterium tumefaciens*. *mBio* **6**, e00156 (2015).
571 10. J. Xu *et al.*, Genetic analysis of *Agrobacterium tumefaciens* unipolar
572 polysaccharide production reveals complex integrated control of the motile-to-

573 sessile switch. *Mol Microbiol* **89**, 929-948 (2013).
574 11. M. Labine *et al.*, Enzymatic and mutational analysis of the PruA pteridine
575 reductase required for pterin-dependent control of biofilm formation in
576 *Agrobacterium tumefaciens*. *J Bacteriol* 10.1128/JB.00098-20 (2020).
577 12. N. Feirer, C. Fuqua, Pterin function in bacteria. *Pteridines* **28**, 23-36 (2017).
578 13. J. M. Green, B. P. Nichols, R. G. Matthews, "Folate biosynthesis, reduction and
579 polyglutamylation" in *Escherichia coli* and *Salmonella*: Cellular and Molecular
580 Biology, F. C. Neidhardt, Ed. (ASM Press, Washington, D.C., 1996), vol. 1, chap.
581 41, pp. 665-673.
582 14. S. Leimkuhler, M. M. Wuebbens, K. V. Rajagopalan, The history of the discovery
583 of the molybdenum cofactor and novel aspects of its biosynthesis in bacteria.
584 *Coord Chem Rev* **255**, 1129-1144 (2011).
585 15. A. Pribat *et al.*, FolX and FolM are essential for tetrahydromonapterin synthesis
586 in *Escherichia coli* and *Pseudomonas aeruginosa*. *J Bacteriol* **192**, 475-482
587 (2010).
588 16. G. J. Workun, K. Moquin, R. A. Rothery, J. H. Weiner, Evolutionary persistence
589 of the molybdopyranopterin-containing sulfite oxidase protein fold. *Microbiol. Mol.*
590 *Biol. Rev.* **72**, 228-248 (2008).
591 17. C. Kisker *et al.*, A structural comparison of molybdenum cofactor-containing
592 enzymes. *FEMS Microbiol Rev* **22**, 503-521 (1998).
593 18. V. R. Sokya, W. Pfleiderer, R. Prewo, Pteridines: Synthesis and characteristics of
594 5,6-dihydro-6-(1,2,3-trihydroxypropyl)pteridines: Covalent intramolecular
595 adducts. *Helv. Chim. Acta.* **73**, 808-826 (1990).
596 19. C. Manoil, J. J. Mekalanos, J. Beckwith, Alkaline phosphatase fusions: sensors
597 of subcellular location. *J Bacteriol* **172**, 515-518 (1990).
598 20. H. Nielsen, K. D. Tsirigos, S. Brunak, G. von Heijne, A brief history of protein
599 sorting prediction. *Protein J* **38**, 200-216 (2019).
600 21. S. Okuda, H. Tokuda, Lipoprotein sorting in bacteria. *Annu Rev Microbiol* **65**,
601 239-259 (2011).
602 22. D. Huber *et al.*, Use of thioredoxin as a reporter to identify a subset of
603 Escherichia coli signal sequences that promote signal recognition particle-
604 dependent translocation. *J Bacteriol* **187**, 2983-2991 (2005).
605 23. C. F. Schierle *et al.*, The DsbA signal sequence directs efficient, cotranslational
606 export of passenger proteins to the *Escherichia coli* periplasm via the signal
607 recognition particle pathway. *J Bacteriol* **185**, 5706-5713 (2003).
608 24. S. Beyhan, L. S. Odell, F. H. Yildiz, Identification and characterization of cyclic
609 diguanylate signaling systems controlling rugosity in *Vibrio cholerae*. *J Bacteriol*
610 **190**, 7392-7405 (2008).
611 25. L. Loschi *et al.*, Structural and biochemical identification of a novel bacterial
612 oxidoreductase. *J Biol Chem* **279**, 50391-50400 (2004).
613 26. J. A. Ronau *et al.*, A conserved acidic residue in phenylalanine hydroxylase
614 contributes to cofactor affinity and catalysis. *Biochemistry* **53**, 6834-6848 (2014).
615 27. C. Chen *et al.*, Structural basis for molecular recognition of folic acid by folate
616 receptors. *Nature* **500**, 486-489 (2013).
617 28. A. S. Wibowo *et al.*, Structures of human folate receptors reveal biological
618 trafficking states and diversity in folate and antifolate recognition. *Proc Natl Acad*

619 *Sci U S A* **110**, 15180-15188 (2013).
620 29. R. L. Blakley, S. J. Benkovic, *Folates and Pterins: Chemistry and Biochemistry of*
621 *Pterins* (John Wiley & Sons, Inc., 1985), vol. 2.
622 30. K. Iwai, M. Kobashi, H. Fujisawa, Occurrence of *Crithidia* factors and folic acid in
623 various bacteria. *J Bacteriol* **104**, 197-201 (1970).
624 31. A. Noiriel, V. Naponelli, G. G. Bozzo, J. F. Gregory, 3rd, A. D. Hanson, Folate
625 salvage in plants: pterin aldehyde reduction is mediated by multiple non-specific
626 aldehyde reductases. *Plant J* **51**, 378-389 (2007).
627 32. T. Arai *et al.*, Auto-oxidation of 5,6,7,8-tetrahydroneopterin *Pteridines* **9**, 26-28
628 (1988).
629 33. C. Chan *et al.*, Structural basis of activity and allosteric control of diguanylate
630 cyclase. *Proc Natl Acad Sci U S A* **101**, 17084-17089 (2004).
631 34. F. Rao, Y. Yang, Y. Qi, Z. X. Liang, Catalytic mechanism of cyclic di-GMP-
632 specific phosphodiesterase: a study of the EAL domain-containing RocR from
633 *Pseudomonas aeruginosa*. *J Bacteriol* **190**, 3622-3631 (2008).
634 35. A. Ortega, I. B. Zhulin, T. Krell, Sensory repertoire of bacterial chemoreceptors.
635 *Microbiol Mol Biol Rev* **81** (2017).
636 36. J. P. Cerna-Vargas, B. Sanchez-Romera, M. A. Matilla, A. Ortega, T. Krell,
637 Sensing preferences for prokaryotic solute binding protein families. *Microb*
638 *Biotechnol* **16**, 1823-1833 (2023).
639 37. A. A. Bridges, J. A. Prentice, C. Fei, N. S. Wingreen, B. L. Bassler, Quantitative
640 input-output dynamics of a c-di-GMP signal transduction cascade in *Vibrio*
641 *cholerae*. *PLoS Biol* **20**, e3001585 (2022).
642 38. E. Karatan, T. R. Duncan, P. I. Watnick, NspS, a predicted polyamine sensor,
643 mediates activation of *Vibrio cholerae* biofilm formation by norspermidine. *J*
644 *Bacteriol* **187**, 7434-7443 (2005).
645 39. A. A. Bridges, B. L. Bassler, Inverse regulation of *Vibrio cholerae* biofilm
646 dispersal by polyamine signals. *Elife* **10** (2021).
647 40. S. R. Cockerell *et al.*, *Vibrio cholerae* NspS, a homologue of ABC-type
648 periplasmic solute binding proteins, facilitates transduction of polyamine signals
649 independent of their transport. *Microbiology* **160**, 832-843 (2014).
650 41. B. Lim, S. Beyhan, F. H. Yildiz, Regulation of Vibrio polysaccharide synthesis
651 and virulence factor production by CdgC, a GGDEF-EAL domain protein, in
652 Vibrio cholerae. *J Bacteriol* **189**, 717-729 (2007).
653 42. D. G. Ha, M. E. Richman, G. A. O'Toole, Deletion mutant library for investigation
654 of functional outputs of cyclic diguanylate metabolism in *Pseudomonas*
655 *aeruginosa* PA14. *Appl Environ Microbiol* **80**, 3384-3393 (2014).
656 43. K. Eilers *et al.*, Phenotypic and integrated analysis of a comprehensive
657 *Pseudomonas aeruginosa* PAO1 library of mutants lacking cyclic-di-GMP-related
658 genes. *Front Microbiol* **13**, 949597 (2022).
659

660 **FIGURE LEGENDS**

661 **Figure 1. PruR binds pterins and is required to control both the DGC and PDE**
662 **activity of DcpA. (A)** PruA reaction and relevant pterin molecule structures. (i): PruA
663 uses NADPH as a cofactor and catalyzes the reduction of a 7,8-dihydropterin substrate
664 to a 5,6,7.8-tetrahydropterin. Atoms are numbered in the dihydropterin. R indicates side
665 groups as shown in (ii)-(iv); (ii): R1- monapterin; (iii): R2- neopterin; (iv): R3 - *p*ABA-
666 glutamate (folate). **(B)** *In vitro* pterin binding assays were performed as described in the
667 supplemental methods with purified Δ_{SS}-PruR (50 μM), NADPH, and with or without
668 His_6-PruA. HPLC fractioned reactions were examined by fluorescence for the oxidized
669 pterins (excitation: 356 nm, emission: 450 nm). UV absorbance at 283 nm was used to
670 measure folate relative to standards. PruR was incubated with the following pterin or
671 folate species: H_2MPt, dihydromonapterin; H_4MPt, PruA-generated-
672 tetrahydromonapterin; H_2NPt, dihydroneopterin; H_4NPt, PruA-generated
673 tetrahydroneopterin; H_2F, dihydrofolate; and H_4F, tetrahydrofolate. Bars are averages of
674 triplicate assays with error bars as standard deviations. Analyzed by standard one-way
675 ANOVA and post-hoc Tukey analysis (*P* values relative to H_4MPt, *, <0.05, *** <0.001,
676 ****, <0.0001). **(C)** Biofilm assays of. *A. tumefaciens* C58 WT (gray bar), a Δ*dcpA*
677 mutant (black bars) or a Δ*dcpA*Δ*pruR* double mutant (white bars) containing the vector
678 control or a plasmid-borne P_{lac}-*dcpA* fusion expressing either the wild type *dcpA* or
679 catalytic site mutants (DGC^-, E308A; PDE^-, E431A; DGC^-PDE^-, both). Ratio of acetic
680 acid-solubilized CV absorbance (A_{600}) from 48 h biofilm assays normalized to the OD_{600}
681 planktonic turbidity from the same culture. Assays performed in triplicate and error bars
682 are standard deviation; *P* values calculated comparing complementation of *dcpA* in the

683 Δ*dcpA* strain compared to the Δ*dcpA*Δ*pruR* strain by standard two-tailed *t*-test. *(P*

684 values, * <0.05, **** <0.0001.)

685

686 **Figure 2. PruR is a periplasmic protein. (A)** Signal P prediction of the PruR N-

687 terminal signal sequence. Black arrow, predicted signal peptidase cleavage site; Grey

688 arrow, putative cleavage and lipidation site; Grey text, predicted lipidated Cys19. **(B)**

689 Western blot of SDS-PAGE using α-PruR polyclonal antisera to probe extracts of wild

690 type *A. tumefaciens* C58 WT and the Δ*pruR* mutant on its own or expressing either the

691 P_{lac}-*pruR* plasmid or the P_{lac}-Δ_{SS}*pruR* plasmid (both plasmids also expressing *dcpA*).

692 Cultures were grown to similar densities with or without induction with 400 μM IPTG and

693 fractionated to separate the cytoplasmic/membrane fraction (C lanes) from the

694 periplasmic fraction (P lanes). **(C)** Biofilm assays of WT or a Δ*pruR* mutant derivative

695 with the empty vector plasmid (-) or harboring a plasmid-borne P_{lac} fusion expressing

696 either *pruR* or the Δ_{SS}*pruR* (both plasmids also express *dcpA*). Ratio of acetic acid-

697 solubilized CV A_{600} from 48 h biofilm assays normalized to the OD_{600} planktonic turbidity

698 of the same culture. Assays performed in triplicate and error bars are standard

699 deviation; *P* values calculated by standard two-tailed *t*-test (*P* values, *** <0.01).

700

701 **Figure 3. PruR forms a complex with the periplasmic region of DcpA. (A)** Western

702 blot probing for PruR with α–PruR polyclonal antisera . Whole cell suspensions were

703 either untreated or incubated with DSS crosslinker (0.75 mM) for wild type *A.*

704 *tumefaciens* C58 and the Δ*dcpA* mutant. Wild type *A. tumefaciens* harboring a plasmid

705 ectopically expressing either *pruR-dcpA* or *pruA* from P_{lac} (400 μM IPTG) was also

706 subjected to same analysis. Black arrows; PruR-DcpA complex, 87 kDa; DcpA, 71 kDa;
707 PruR; 16 kDa. **(B)** Similar western blot to panel A probing for PruR following DSS
708 crosslinking of whole cell suspensions of either *A. tumefaciens* wild type strain or the
709 Δ*dcpA* mutant. Either the cytoplasmic ($DcpA_{cyt}$) or periplasmic ($DcpA_{peri}$) domains of
710 DcpA are ectopically expressed from P_{lac} (400 μM IPTG). Red triangles, PruR-DcpA, 87
711 kDa; Blue triangles, expected size of PruR-$DcpA_{cyt}$, ~68 kDa; Black triangles, PruR-
712 $DcpA_{peri}$,38 kDa. α-PruR used at 1:40,000 and antibody binding detected with GAR-
713 HRP secondary antibody and chemiluminescent substrate on a BioRad ChemiDoc.
714 Non-specific bands serve as protein loading controls.
715
716 **Figure 4. Deletion of *pruA* diminishes the interaction between DcpA and PruR.**
717 Western blot probing for the PruR-$DcpA_{peri}$ complex following *in vivo* DSS crosslinking in
718 *A. tumefaciens* wild type or a Δ*pruA* mutant expressing the P_{lac}-*pruR-dcpA*$_{cyt}$ plasmid
719 (400 μM IPTG). Probed with polyclonal antibody preparations **(A)** α-PruR, 1:40,000; **(B)**
720 α-$DcpA_{peri}$, 1:20,000. Antibody binding was detected with GAR-HRP secondary antibody
721 and a chemiluminescent substrate on a BioRad ChemiDoc. Non-specific bands serve
722 as protein loading controls.
723
724 **Figure 5. The *pruR-dcpA* operon is conserved across Proteobacteria in animal**
725 **and human pathogens. (A)** Domain structure for PruR and DcpA; transmembrane
726 domains and signal sequence are black lines; DGC domain is green; PDE domain is
727 lime green; Pt indicates the pterin-binding activity of the protein. **(B)** Presumptive
728 operon structure for homologs of the *pruR-dcpA* operon from multiple pathogens. A

729 subset of DcpA homologs are truncated relative to DcpA, and contain only the DGC
730 domain. *Ochrobactrum anthropi* ATCC 49188, *Klebsiella pneumoniae pneumoniae*
731 ATCC 700721; *Vibrio cholerae,* O1 biovar El Tor str. N16961*; Vibrio vulnificus* CMCP6;
732 *Pseudomonas aeruginosa* PA01. Color coding as in panel A – gene and domain sizes
733 are proportional.
734
735 **Figure 6. The structure of PruR is a degenerate SUOX fold conserved in multiple**
736 **Alpha- and Gammaproteobacteria (A)** The overall structure of PruR from *A.*
737 *tumefaciens* is depicted. The secondary structure elements are labeled and shown in
738 red (α helices), yellow (β-strands) and green (loops). **(B)** Superposition of PruR from *A.*
739 *tumefaciens* (orange, 7kos; violet, 7kou), *K. pneumoniae* (pink, 7rkb) *V. cholerae*
740 *(*wheat, 7kp2), *V. vulnificus* (light green, 7kom)*.* The peptide main chains of all
741 structures are depicted as ribbons. **(C)** Multiple sequence alignment of PruR proteins
742 with secondary structure elements from *A. tumefaciens* (PDB code 7kos) mapped
743 above. Lime green circles mark pterin binding site residues conserved across all
744 proteins.
745
746 **Figure 7. Comparison of PruR structure to conserved MoCo-binding domains. (A)**
747 Superposition of *A. tumefaciens* PruR (orange, 7kou) with the MoCo binding domain of
748 chicken liver SUOX (violet, PDB 1sox) and *E. coli* YedY (salmon, PDB 1xdq). The
749 MoCo and conserved C185 of SUOX are shown as balls-and-sticks (carbon, violet;
750 oxygen, red; nitrogen, dark blue; sulfur, yellow), the molybdenum is shown as a green
751 sphere, water molecules as small cyan spheres and hydrogen bonds as black, dashed
752 lines. W70, conserved in PruR, is also shown as sticks. **(B)** Multiple sequence

753 alignment of *A. tumefaciens* PruR with the MoCo binding domain of chicken liver sulfite
754 oxidase and *E. coli* YedY. The magenta oval marks PruR W70 that aligns with the
755 conserved **C185** in canonical MoCo-binding domains. The green oval marks an active
756 site tyrosine conserved in pterin-binding proteins. **(C)** A zoomed in view of superposition
757 of *A. tumefaciens* (orange, 7kou) and *K. pneumoniae* (pink, 7rkb) PruR. The neopterin
758 and conserved residues of the pterin binding pocket are shown as sticks. Residue
759 sidechains are numbered according to *A. tumefaciens*. **(D)** Superposition of all observed
760 neopterin binding modes from crystal structures of *K. pneumoniae* (7RKB) and *V.*
761 *cholerae* (7KP2). The binding pocket is represented as an electrostatic surface potential
762 (blue-to-red, positive-to-negative charge) and neopterin as stick models. Carbons are in
763 yellow (alternative conformation A, *V. cholerae*), grey (alternative conformation B, *V.*
764 *cholerae*, 7kp2) and green (*K. pnuemoniae*, 7rkb), with oxygen in red and nitrogen in
765 blue.

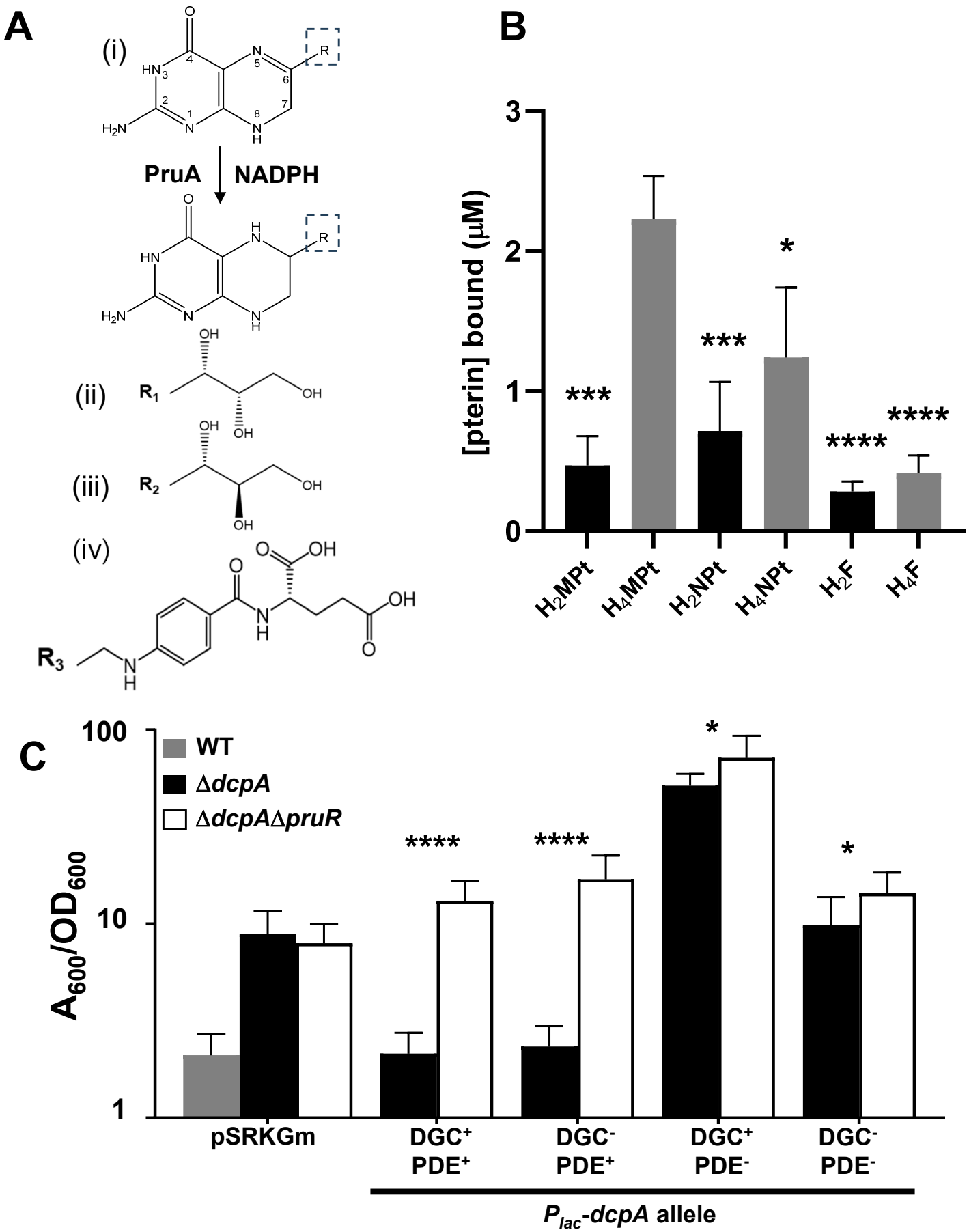

Figure 1 – PruR-DcpA

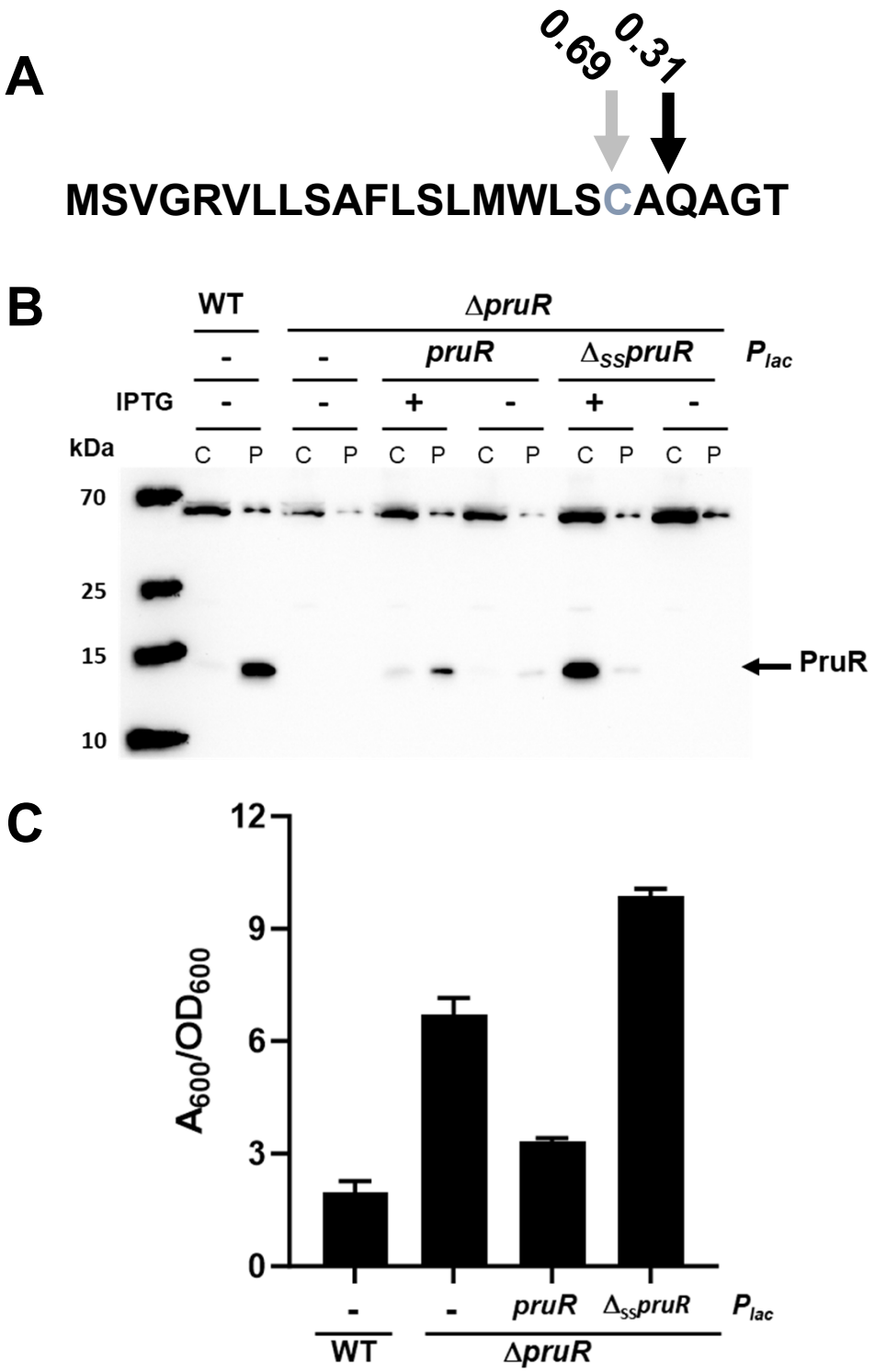

Figure 2 – PruR-DcpA

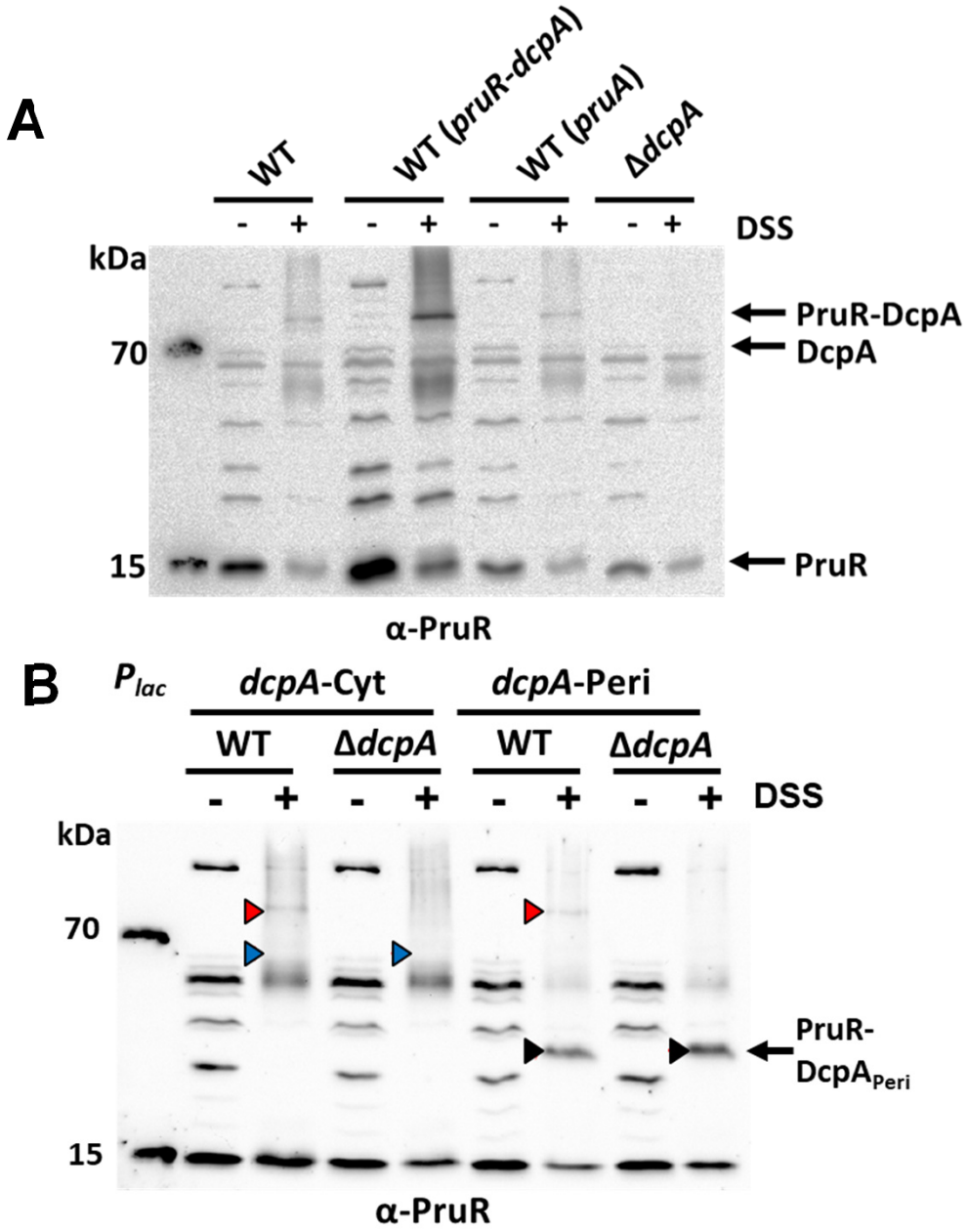

Figure 3 – PruR-DcpA

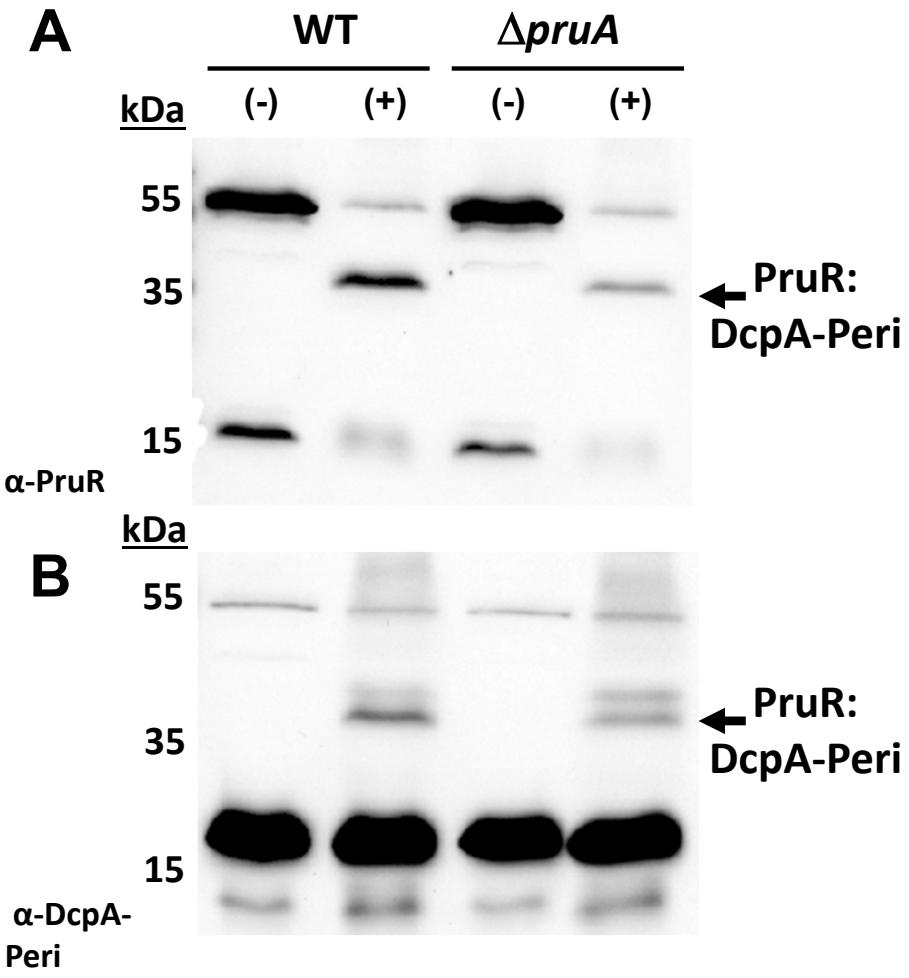

Figure 4 - PruR-DcpA

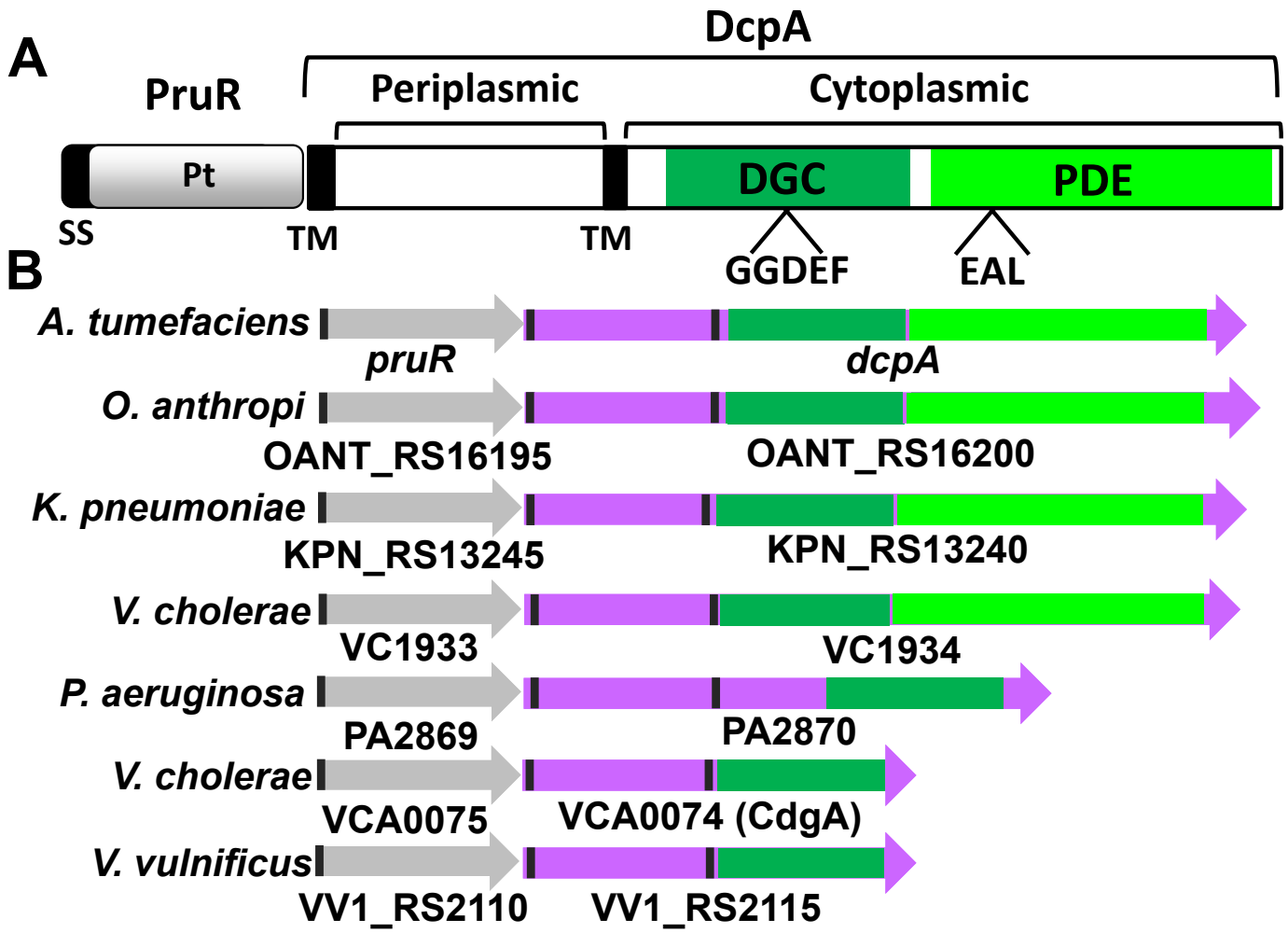

Figure 5 - PruR-DcpA

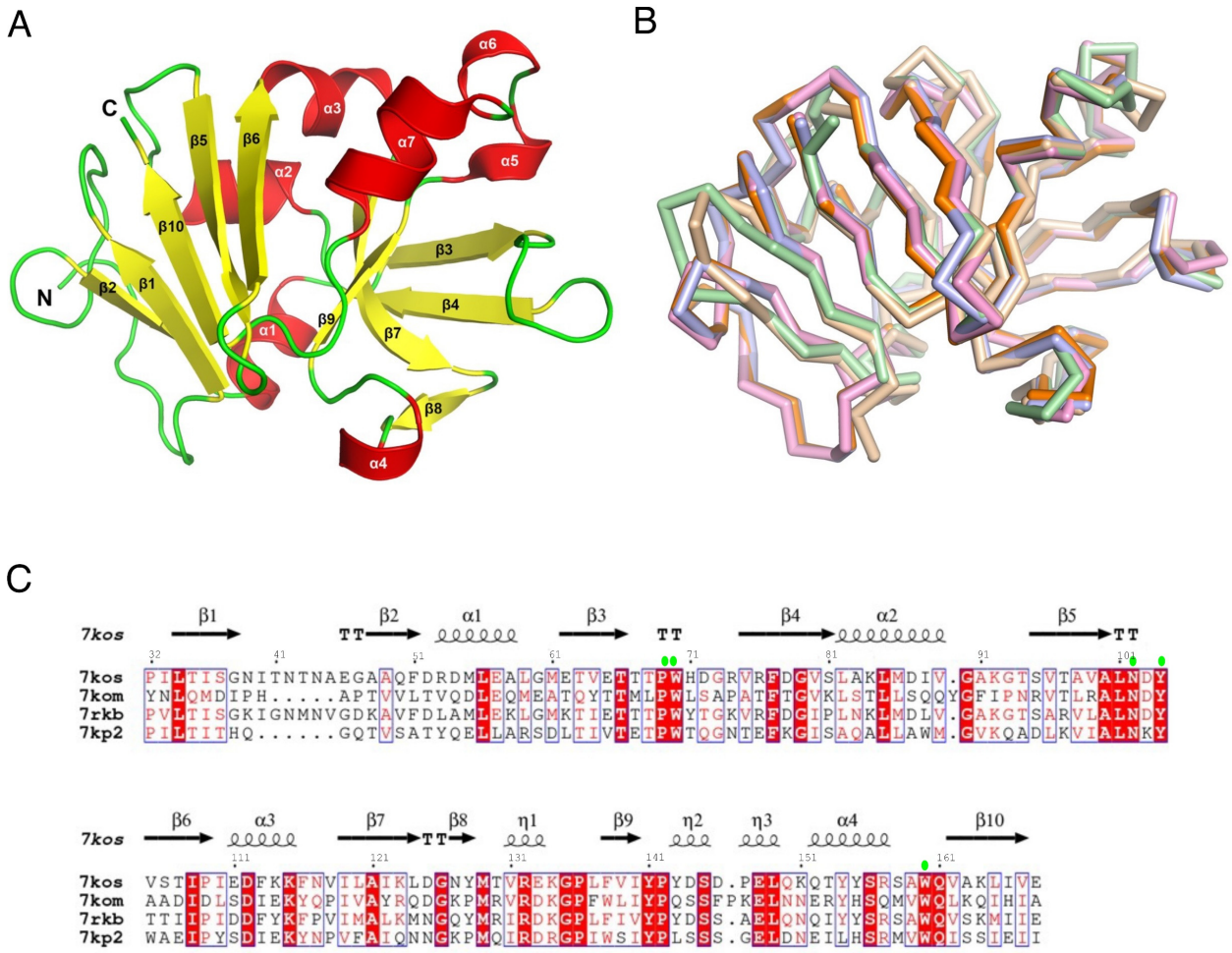

Figure 6 - PruR-DcpA

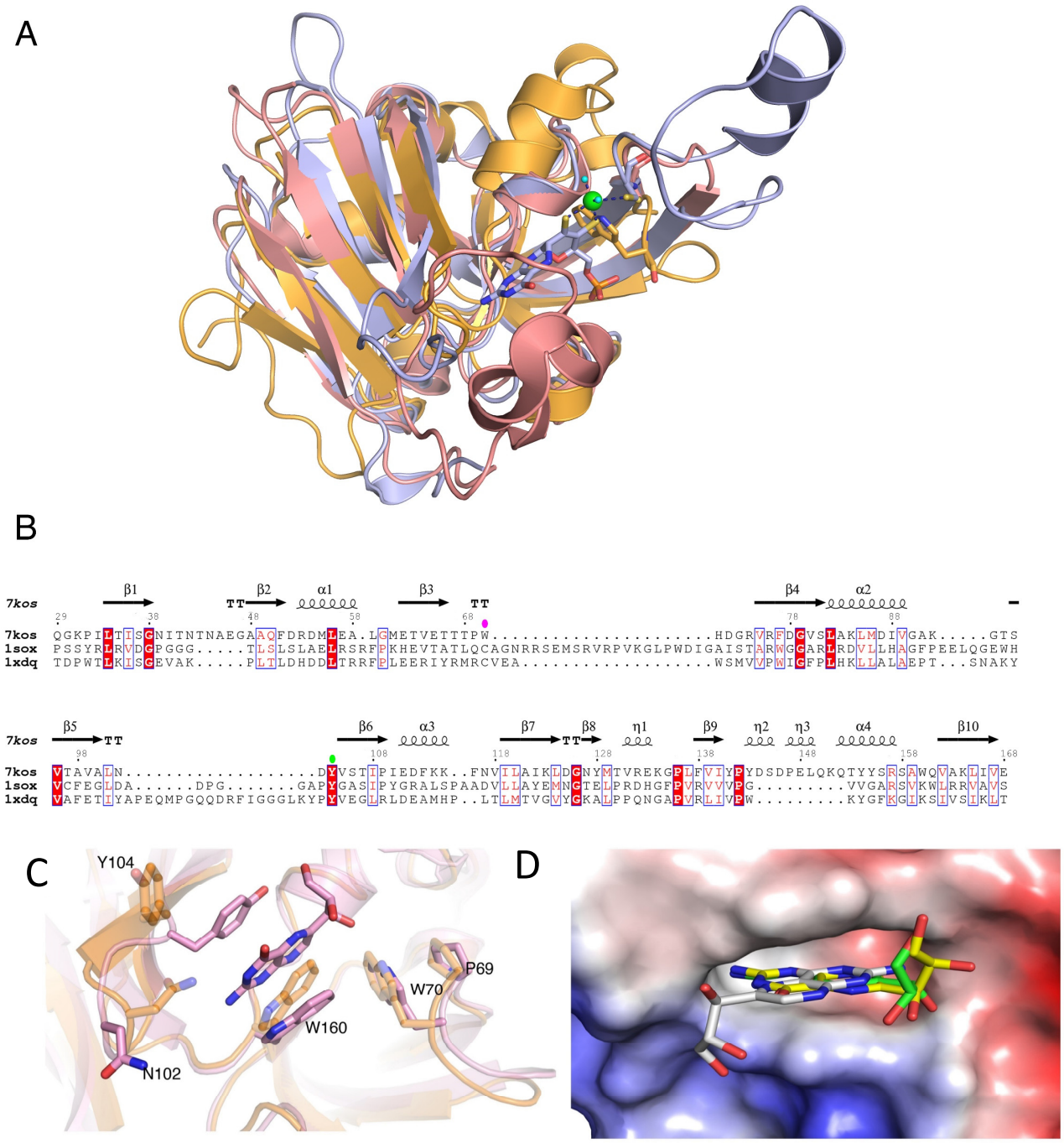

Figure 7 - PruR-DcpA